Expanded View Figures

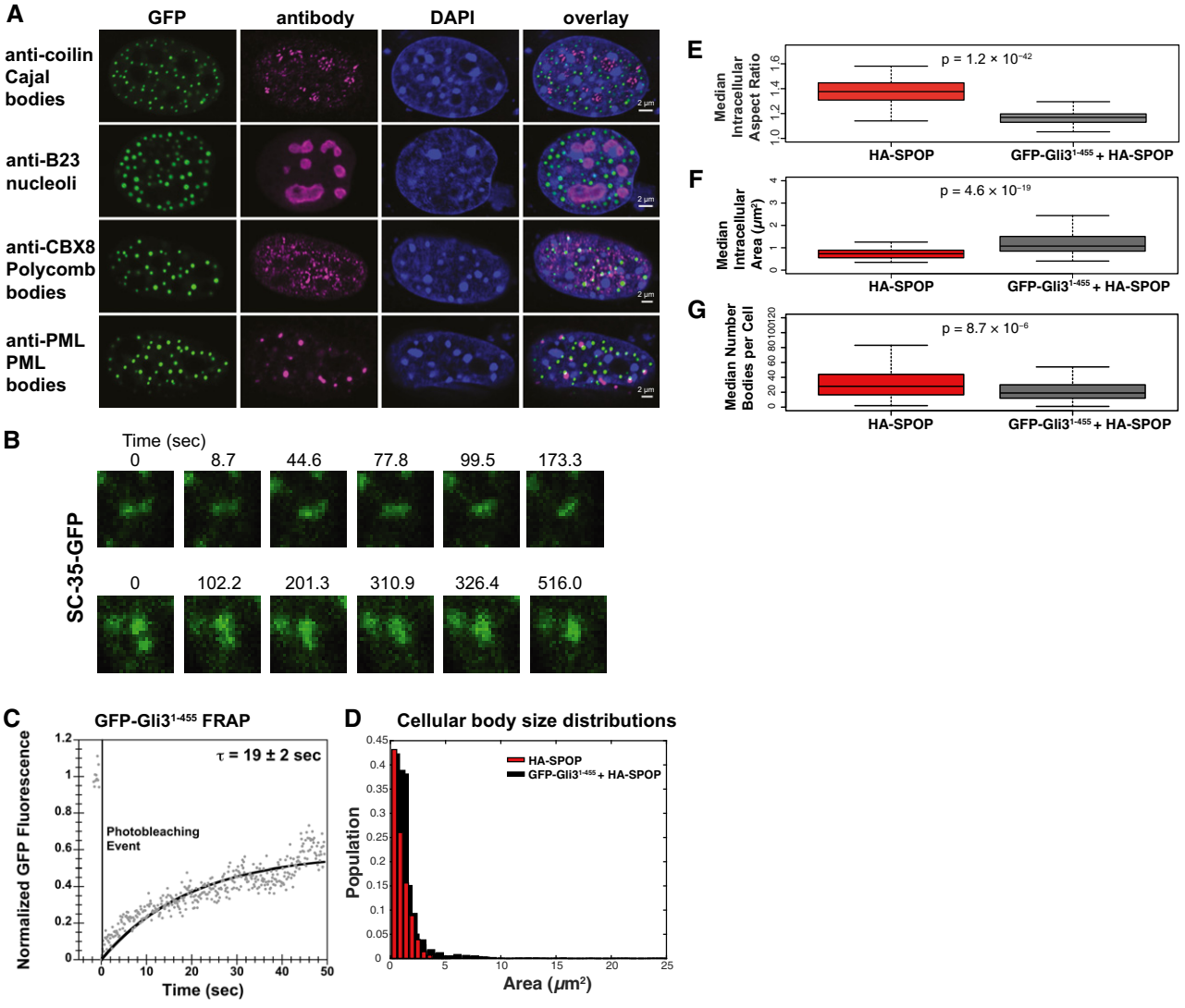

Figure EV1. Size distribution of nuclear puncta.

A $Gli3^{1–455}$-positive bodies are not Cajal bodies, nucleoli, polycomb bodies, or PML bodies. NIH 3T3 cells were transfected with GFP-$Gli3^{1–455}$ and stained with antibodies against coilin (a Cajal marker), B23 (a nucleolus marker), CBX8 (a polycomb marker), or PML (a PML body marker).

B NIH 3T3 cells were transfected with a construct expressing SC-35-GFP and GFP fluorescence was monitored in live cells. Snapshots at indicated time points show a nuclear speckle fusion event.

C NIH 3T3 cells were transfected with a construct expressing GFP-$Gli3^{1–455}$, and GFP fluorescence was monitored in live cells. Individual nuclear bodies were photobleached, and FRAP was monitored for 1 min. Data were normalized to the maximum and minimum intensity. The mean characteristic recovery time is indicated ± SEM.

D Histograms depicting the size distribution of nuclear body areas are shown for cells transfected with HA-SPOP alone and GFP-$Gli3^{1–455}$ + HA-SPOP.

E–G NIH 3T3 cells were transfected with only HA-SPOP or GFP-$Gli3^{1–455}$ + HA-SPOP. Box plots of the median aspect ratio of the (E) GFP-$Gli3^{1–455}$-positive nuclear bodies in one cell, (F) of the intracellular median area of nuclear speckles, and (G) of the number of bodies per cell for cells transfected with HA-SPOP alone and GFP-$Gli3^{1–455}$ + HA-SPOP are shown. All three were significantly different ($P = 1.2 \times 10^{-42}$, $P = 4.6 \times 10^{-19}$, and $P = 8.7 \times 10^{-6}$, respectively, according to the Wilcoxon rank-sum test), consistent with the different nature of distinct nuclear bodies. The medians are indicated as black horizontal lines within the boxes, and boxes enclose values between the first and third quartile. Interquartile range (IQR) is calculated by subtracting the first quartile from the third quartile. All values that lay more than 1.5× IQR lower than the first quartile or 1.5× higher than the third quartile are outliers that are plotted as squares. The smallest and highest values that are not outliers are connected with the dashed line.

Source data are available online for this figure.

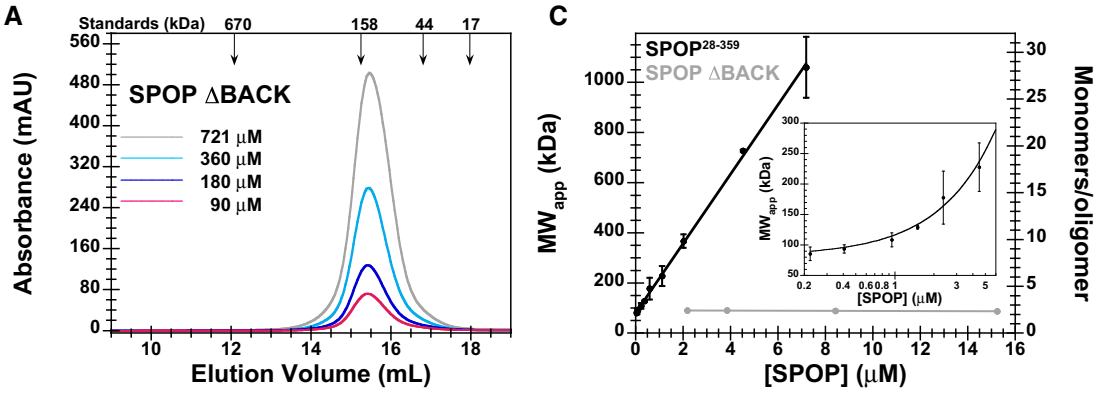

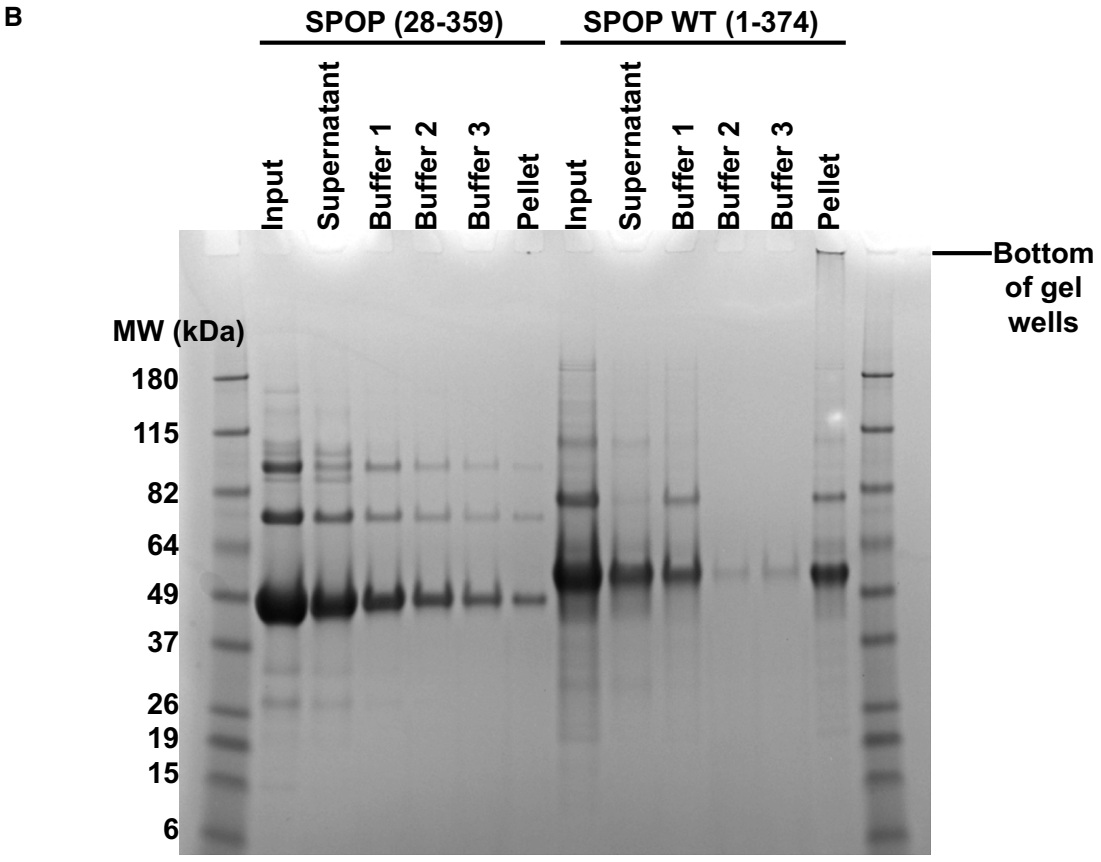

Figure EV2. SPOP ΔBACK does not elute in a concentration-dependent manner and SPOP WT forms aggregates *in vitro*.

A SEC chromatograms of given loading concentrations of SPOP ΔBACK are shown. The concentrations were normalized to the monomer molecular weight, that is, identical concentrations of dimeric SPOP ΔBACK and oligomeric SPOP$^{28–359}$ contain identical numbers of protomers.

B Protein aggregation was assayed by centrifuging protein samples, resuspending soluble pelleted material in buffer three times, and then resuspending the final insoluble pellet in sample loading dye. The ultracentrifugation conditions are expected to pellet some of the larger SPOP$^{28–359}$ oligomeric species. These species are readily soluble in fresh buffer and do not represent aggregated material. In contrast, the majority of SPOP FL forms insoluble aggregates that do not dissociate even under extensive dilution, but can be resolubilized in denaturing gel sample buffer. These results show at least very slow off-rates of SPOP from the aggregates, not only high stability of the aggregates, and are therefore strongly indicative of poor reversibility of aggregation.

C SPOP$^{28–359}$ oligomers have no apparent size limit. The apparent molecular weights (calculated from globular standards) of the major eluting species for each injection in Fig 4A and panel (A) are plotted against their elution concentrations and fit to a line. The number of monomers per oligomer was calculated by dividing the apparent molecular weight by the monomer mass and assumes regular packing of the monomer in the oligomer. The average and standard deviation of two independent experiments are shown for SPOP$^{28–359}$. Inset shows the same data in a semi-logarithmic plot to highlight the lower concentrations of SPOP$^{28–359}$ assayed.

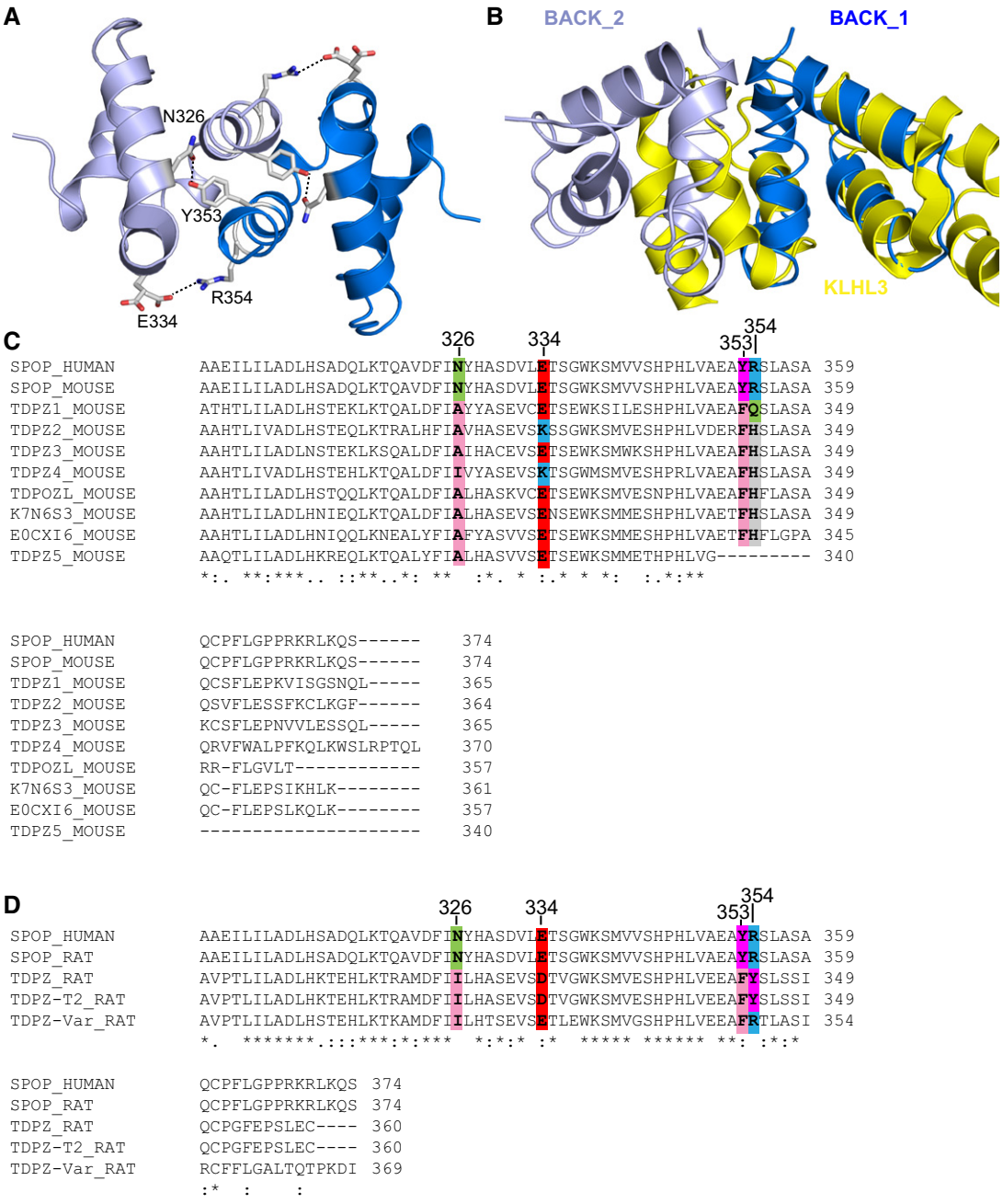

Figure EV3. A family of BTB–BACK domain-containing proteins in rodents may self-associate isodesmically.

A The BACK domain dimer is stabilized via a hydrogen bond between N326 and Y353 and a salt bridge between E334 and R354. The two BACK domain monomers are shown in different shades of blue.

B The long form of the BACK domain, as exemplified by KLHL3 (shown in yellow, PDB ID 4HXI), occludes the dimerization interface of the short SPOP BACK domain.

C, D The human genome contains only two genes encoding a protein with a BTB and short version of the BACK domain, SPOP and SPOPL, the latter of which does not dimerize because of a sterically hindering insertion. The family of BTB–BACK domain-containing proteins is expanded in rodents. (C) Alignment of mouse protein sequences containing a BTB and a short BACK domain with human SPOP. The N326/Y353 and E334/R354 interactions are not conserved but could potentially be replaced by hydrophobic/aromatic and negatively charged/histidine interactions, respectively. (D) Alignment of rat protein sequences containing a BTB and a short BACK domain with human SPOP. In the TDPZ variant shown on the bottom, residues E334 and R354 are conserved, potentially enabling a salt bridge. This protein may undergo isodesmic self-association into higher-order oligomers.

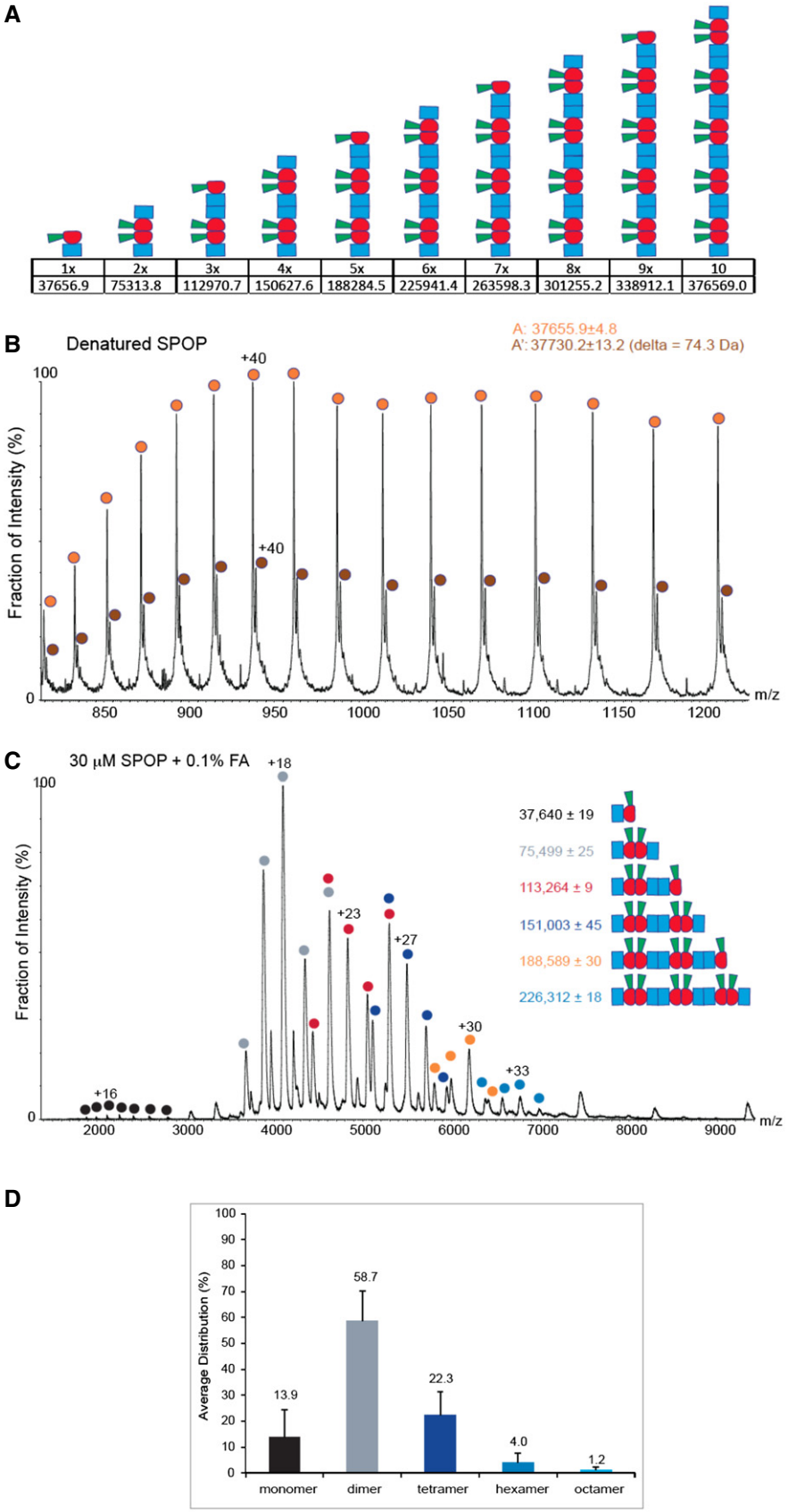

Figure EV4. Detailed MS analysis of SPOP oligomers.

A Schematic representation of putative SPOP assemblies. Under each assembly state, the number of monomers and the theoretical mass are shown.

B Mass spectrum of denatured SPOP. To evaluate the purity of the sample, SPOP (50 pmol) was loaded onto a monolithic column (Rozen *et al*, 2013) and eluted in a linear gradient of 20–50% ACN over 30 min. The protein eluted as a single peak at 17.6–19.8 min, at approximately 33% ACN. The spectrum shows a major population of 37,656 ± 5 Da (orange circles) and a smaller population of 37,730 ± 13 Da (brown circles). The mass difference may result from β-mercaptoethanol.

C MS spectrum of SPOP assemblies under partial denaturing conditions. SPOP was analyzed by performing MS after adding of 0.1% formic acid (30 μM) to disturb the non-covalent interactions. Under these conditions, trimers (red circles) and pentamers (orange circles) were generated. The fact that odd numbers of assemblies appear only under mild denaturing conditions indicates strong interactions between two monomers.

D Size distribution of SPOP oligomers at 30 μM protomer concentration from seven independent measurements.

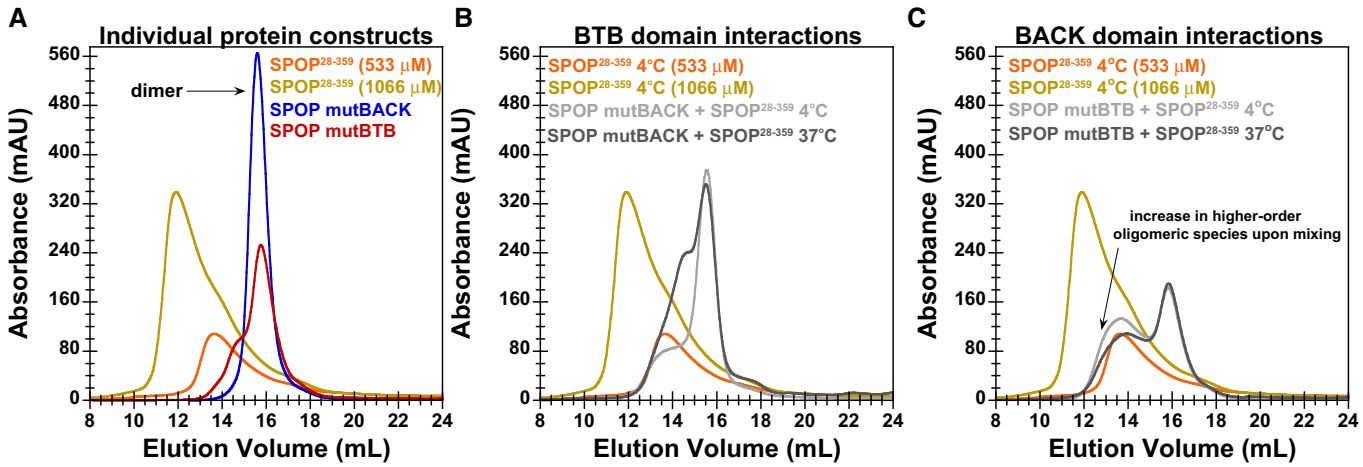

Figure EV5. The dynamic nature of higher-order SPOP oligomers is mediated by the BACK domain.

Samples were either mixed at 4°C and immediately injected onto the column or were incubated at 37°C for 90 min prior to injection. All SEC was performed at 4°C.

A SEC chromatograms for individual SPOP constructs injected at a loading concentration of 533 μM (and $SPOP^{28–359}$ at 1,066 μM) are shown. In agreement with CG-MALS results, SPOP mutBTB and SPOP mutBACK predominantly form dimers (red and blue lines, respectively).

B SEC chromatogram for mixtures of 533 μM $SPOP^{28–359}$ with 533 μM of SPOP mutBACK is shown. When equal amounts of $SPOP^{28–359}$ and one of the mutants were mixed at 4°C, we observed that SPOP mutBACK, which cannot participate in typical BACK–BACK interactions, did not increase the population of higher-order oligomers relative to that of WT only, as evidenced by a similar elution peak from the oligomeric species. This result shows that BTB dimers do not dissociate on the timescale of SEC at low temperature and cannot form hetero-oligomers with $SPOP^{28–359}$. However, incubation at 37°C for 90 min renders BTB domain interactions dynamic enough to allow for BTB domain-mediated exchange between WT and SPOP mutBACK (dark gray line). The hetero-oligomers are smaller in size than oligomeric species observed for $SPOP^{28–359}$ alone at 533 μM (orange line).

C SEC chromatogram for mixtures of 533 μM $SPOP^{28–359}$ with 533 μM of SPOP mutBTB is shown. Conversely, in mixtures of $SPOP^{28–359}$ and SPOP mutBTB, which can effectively interact only through the BACK domain, the population of the higher-order oligomeric species increased relative to that of $SPOP^{28–359}$ alone, irrespective of incubation time or temperature (gray lines). However, the mixed oligomers are smaller than $SPOP^{28–359}$ oligomers at an equimolar protein loading concentration (golden line).

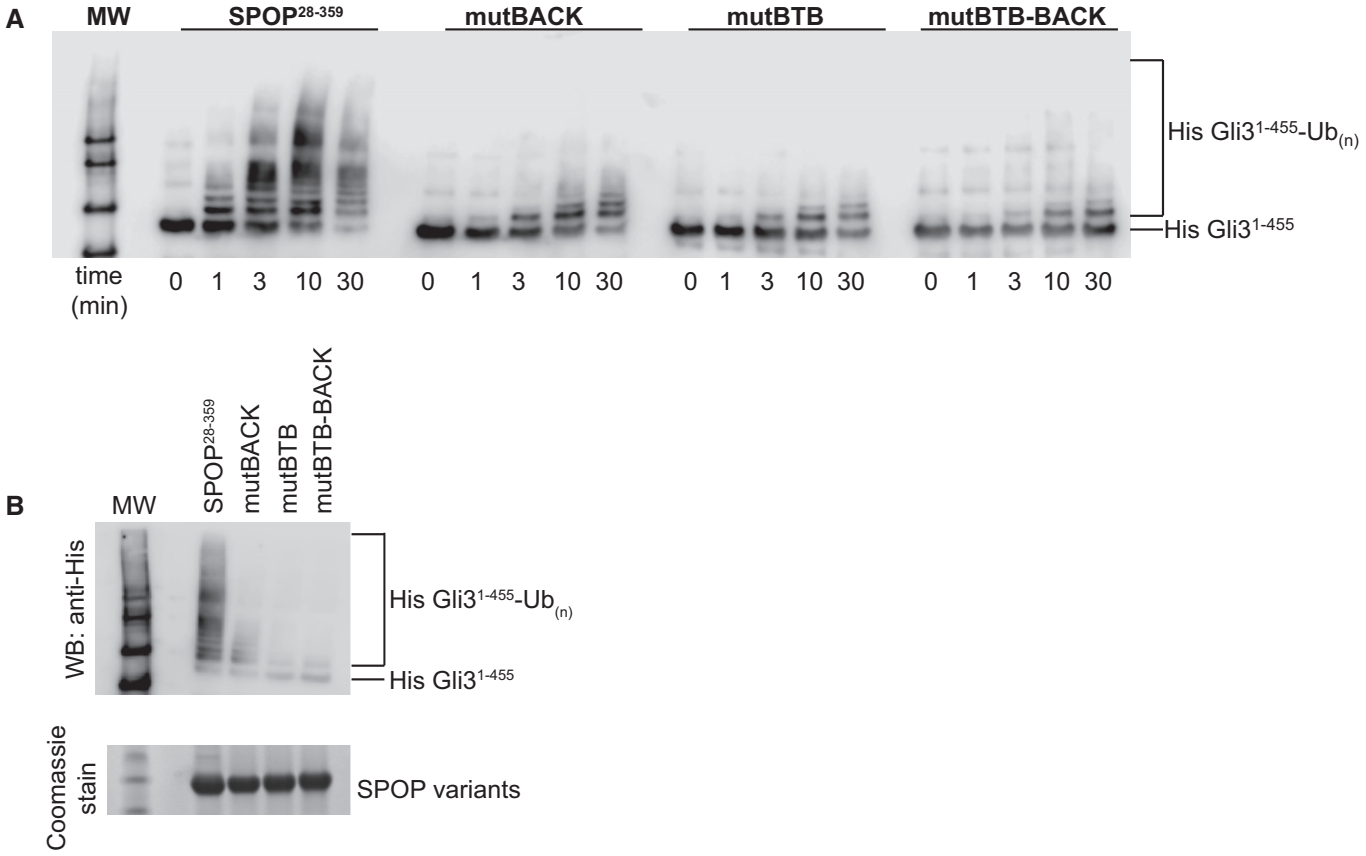

Figure EV6. Higher-order SPOP self-association promotes ubiquitination *in vitro*.

A *In vitro* ubiquitination assays with $CRL3^{SPOP}$ were performed as described previously (Zhuang *et al*, 2009) using His-$Gli3^{1-455}$ as a substrate, $SPOP^{28-359}$, and each of the self-association-incompetent mutants. The reaction was monitored for 30 min, and time points taken are indicated below the Western blot. Ubiquitination efficiency was monitored by immunoblotting with an anti-His antibody.

B Reactions were performed as in (A) and monitored for 30 min. Equal amounts of SPOP variants were used as shown in the SDS–PAGE gel.